Quasi-1D TiS_3 Nanoribbons: Mechanical Exfoliation and Thickness-Dependent Raman Spectroscopy

*Alexey Lipatov,[1] Michael J. Loes,[1] Haidong Lu,[2] Jun Dai,[1] Piotr Patoka,[3] Nataliia S. Vorobeva,[1] Dmitry S. Muratov,[1,4] Georg Ulrich,[3,5] Bernd Kästner,[5] Arne Hoehl,[5] Gerhard Ulm,[5] Xiao Cheng Zeng,[1,6] Eckart Rühl,[3] Alexei Gruverman,[2,6] Peter A. Dowben,[2,6] Alexander Sinitskii[1,6]**

[1]Department of Chemistry, University of Nebraska, Lincoln, NE 68588, USA

[2]Department of Physics and Astronomy, University of Nebraska, Lincoln, NE 68588, USA

[3]Physical Chemistry, Institut für Chemie und Biochemie, Freie Universität Berlin, 14195 Berlin, Germany

[4]National University of Science and Technology "MISIS", Moscow 119991, Russia

[5]Physikalisch-Technische Bundesanstalt (PTB), Abbestr. 2-12, 10587 Berlin, Germany

[6]Nebraska Center for Materials and Nanoscience, University of Nebraska, Lincoln, NE 68588, USA

KEYWORDS Quasi-one-dimensional materials, transition metal trichalcogenides (TMTCs), Raman spectroscopy, mechanical exfoliation, scanning near-flied optical microscopy.

ABSTRACT

Quasi-one-dimensional (quasi-1D) materials enjoy growing interest due to their unusual physical properties and promise for miniature electronic devices. However, the mechanical exfoliation of quasi-1D materials into thin flakes and nanoribbons received considerably less attention from researchers than conventional layered crystals. In this study, we investigated the micromechanical exfoliation of representative quasi-1D crystals, TiS_3 whiskers, and demonstrate that they typically split into narrow nanoribbons with very smooth, straight edges and clear signatures of 1D TiS_3 chains. The theoretical calculations show that the energies required for breaking weak interactions between the two-dimensional (2D) layers and between 1D chains within the layers are comparable, and in turn are considerably lower than those required for breaking the covalent bonds within the chains. We also emulated macroscopic exfoliation experiments on the nanoscale by applying a local shear force to TiS_3 crystals in different crystallographic directions using a tip of an atomic force microscopy (AFM) probe. In the AFM experiments, it was possible to slide the 2D TiS_3 layers relative to each other as well as to remove selected 1D chains from the layers. We systematically studied the exfoliated TiS_3 crystals by Raman spectroscopy and identified the Raman peaks whose spectral positions were most dependent on the crystals' thickness. These results could be used to distinguish between TiS_3 crystals with thickness ranging from one to about seven monolayers. The conclusions established in this study for the exfoliated TiS_3 crystals can be extended to a variety of transition metal trichalcogenide materials as well as other quasi-1D crystals. The possibility of exfoliation of TiS_3 into narrow (few-nm wide) crystals with smooth edges could be important for the future realization of miniature device channels with reduced edge scattering.

Mechanical exfoliation of layered materials using the simple adhesive tape approach is an important technique for producing high-quality two-dimensional (2D) crystals for research at the interface of materials science and condensed matter physics.[1] The layered materials, such as graphite, a large family of transition metal dichalcogenides, hexagonal boron nitride (h-BN) and many others, are very diverse in terms of their chemical composition and physical properties.[2-4] But what they have in common is that they consist of charge-neutral 2D sheets with strong covalent or ionic bonding between the atoms within the sheets (in two dimensions) and weak interaction between the sheets (in the third dimension).

A different class of solids that shares many similarities with these layered crystals but received considerably less attention are quasi-one-dimensional (quasi-1D) materials.[5-8] Titanium trisulfide (TiS_3) is a representative quasi-1D material. It is an n-type semiconductor with a band gap of about 1 eV.[8-11] It was studied for several decades with regard to its prospects for energy storage applications,[12-14] but recently received a surge of attention due to the theoretical predictions of high electron mobilities[15,16] and promising thermoelectric properties.[14,17,18] The crystal structure of TiS_3 is shown in Figure 1a.[5] Similar to the layered crystals, quasi-1D materials are built through interplay of strong covalent bonds and weak van der Waals-like interactions. However, in TiS_3 and other transition metal trichalcogenide (TMTC) crystals with MX_3 composition (M is a transition metal ion, such as Ti, Zr or Hf; X = S, Se or Te), a basic covalently bound structural unit is not a layer but a 1D chain of MX_3 prisms (Figure 1a).[6-8] The weak van der Waals-like interactions assemble these chains into 2D layers, and then the layers stack into 3D crystals. The 1D chains of TiS_3 crystals can be visualized by transmission electron microscopy (TEM) (Figure 1b,c). They consist of trigonal prisms formed by sulfide (S^{2-}) and disulfide (S_2^{2-}) units with Ti^{4+} in the center. TEM image showing the chains perpendicular to *ab* plane is presented in Figure S4 together with corresponding selected area electron diffraction (SAED).

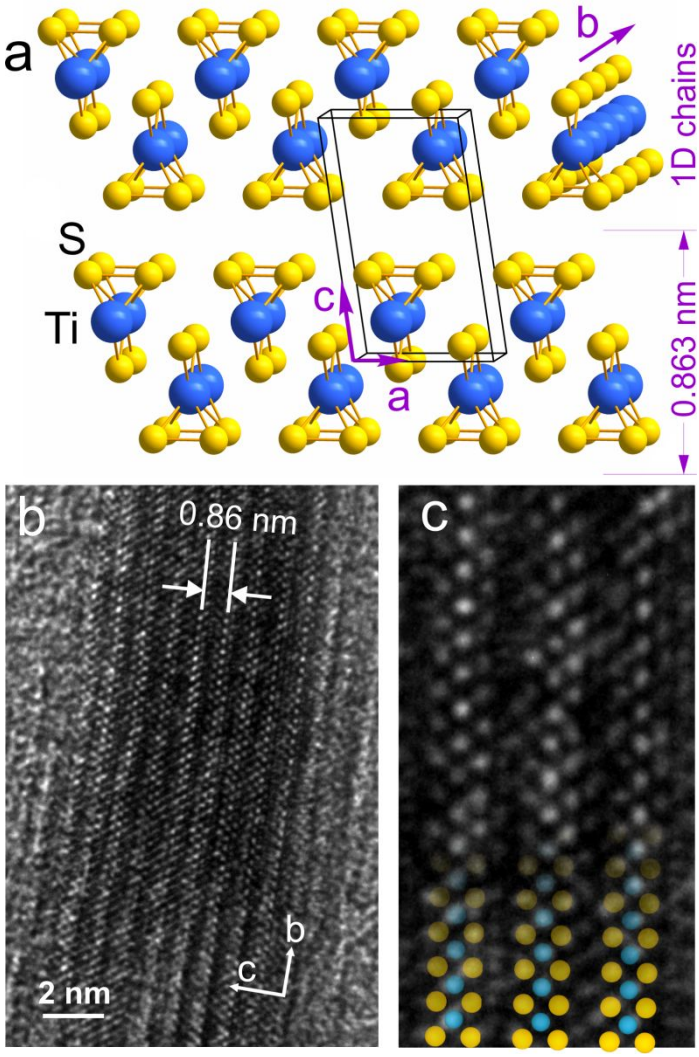

Figure 1. One-dimensional chains in TiS_3 structure. **(a)** Scheme of the monoclinic TiS_3 crystal structure with a P 2_1/m space group and interlayer distance of 0.863 nm. **(b,c)** High-resolution TEM images of a TiS_3 crystal. In (c), the TiS_3 chains are overlaid with blue and yellow circles representing Ti and S atoms, respectively.

TiS_3 crystals can be prepared through a direct reaction between metallic titanium and sulfur vapor at 550 °C (Figure S1),[19,20] and characterized by spectroscopy techniques (Figure S2 and Figure S3). Because of their anisotropic structure, TiS_3 crystals usually grow in a form of whiskers (Figure 2a and

Figure S5) with their long axes corresponding to the crystallographic *b* direction of 1D chains (Figure 1a). Like graphite or similar layered crystals,[1] these TiS_3 whiskers could be placed on an adhesive tape and subjected to micromechanical exfoliation, which was done in a number studies aiming to investigate thin TiS_3 flakes.[21-26] However, while the micromechanical exfoliation is well-established for the layered crystals, it received much less attention for quasi-1D crystals. For TiS_3 and similar crystals, this process is rather peculiar since weak interactions are present in two crystallographic directions, *a* and *c*, and when a mechanical force is applied to a crystal it could split into thinner flakes along both directions.

In this work, we demonstrate that micromechanical exfoliation of quasi-1D crystals (Figure 2b) can produce thin flakes with morphologies very different from those typically observed for the layered crystals with weak interlayer bonding. It was previously reported that because of their quasi-1D structure the TiS_3 crystals typically split into narrow nanoribbons with very smooth and straight edges rather than randomly shaped flakes.[22] We further demonstrate that the surfaces of the exfoliated nanoribbons are not necessarily atomically flat but could bear signatures of the 1D TiS_3 chains. These observations are supported by the theoretical analysis of the cleavage energies for various crystallographic planes in TiS_3 structure. The calculations show that breaking weak bonding interactions between the 2D layers and between 1D chains within the layers require comparable energies, which in turn are considerably lower than those required for breaking the covalent bonds within the chains. We also emulated macroscopic exfoliation experiments on the nanoscale by applying a local shear force to TiS_3 crystals in different crystallographic directions using a tip of an atomic force microscopy (AFM) probe. In the AFM experiments, it was possible to slide the weakly-interacting TiS_3 layers relative to each other as well as to detach the selected 1D chains from the layers. Raman scattering spectroscopy revealed a considerable shift of the frequencies of the two modes in opposite directions with the number of layers, which provides a facile way to determine thicknesses of exfoliated TiS_3 flakes. Finally, we used infrared scattering-type

near-field optical microscopy (s-SNOM) and found suppressions of the substrate phonon responses near the edges of terraces in exfoliated crystals, which is consistent with the uniform sulfur termination of the quasi-1D TiS_3 chains. The conclusions established in this study for the exfoliated TiS_3 crystals can likely be extended to other TMTC materials as well as other quasi-1D crystals.

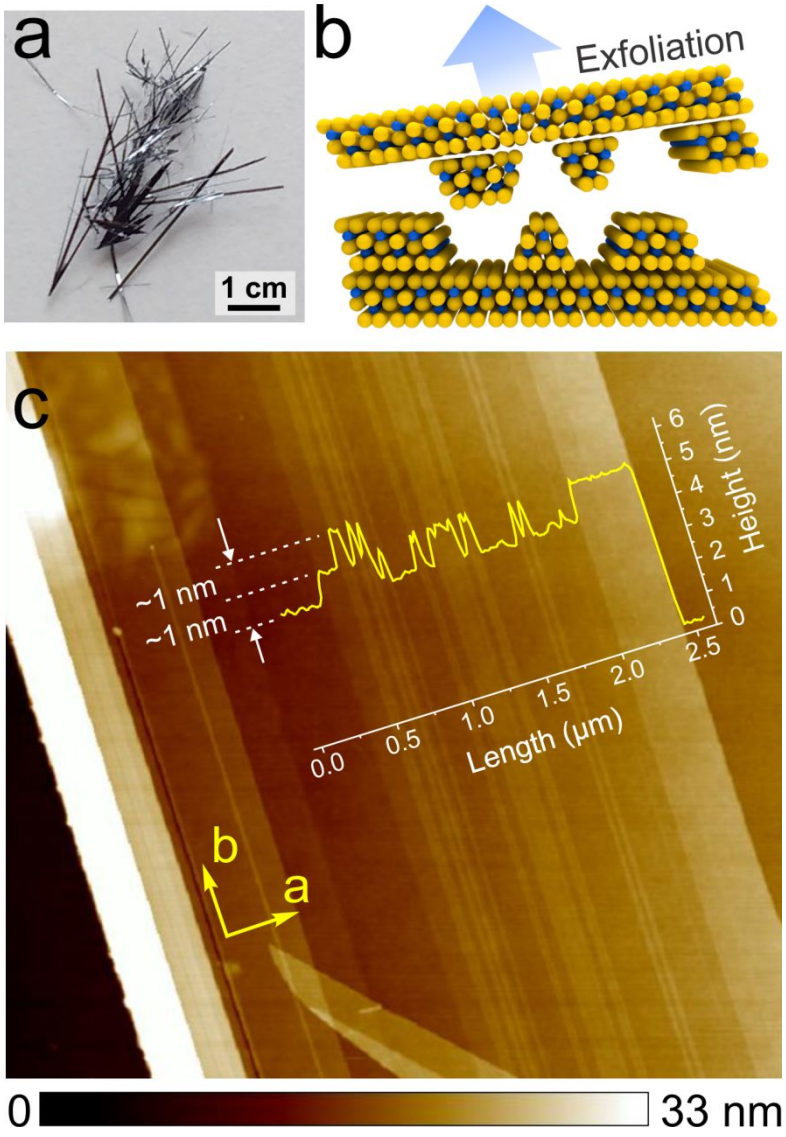

Figure 2. Visualization of one-dimensional chains in TiS_3 whiskers. **(a)** Optical photograph of TiS_3 whiskers. **(b)** Scheme of micromechanical exfoliation of TiS_3. **(c)** AFM image of an exfoliated TiS_3 nanoribbon. Overlaid over the image is the height profile across the nanoribbon.

The peculiarity of the micromechanical exfoliation of TiS_3 crystals can be illustrated by the AFM image in Figure 2c. Unlike exfoliated flakes of graphene, h-BN and other 2D materials, which are normally very flat, the TiS_3 crystals show a structure of parallel stripes that run along the entire length of a crystal. These stripes have very uniform height and widths. The height profile measured across these stripes shows that they exhibit only two height steps of about 1 nm, which correspond precisely to the thickness of a 2D layer in the TiS_3 structure (Figure 1a). Thus, these stripes represent the residual 1D chains of two topmost layers of the exfoliated TiS_3 crystal. The observed uniformity of these stripes suggests that the splitting of these layers likely happened in between the weakly bound chains, as shown in Figure 2b.

In order to support this conclusion, we investigated cleavage energies for different crystallographic planes in the TiS_3 structure. Since the stripes were observed along the crystallographic *b* direction (Figure 2c), we considered several cleavage planes that were parallel to it, as illustrated by Figure 3a. Some of these planes, such as (100), (101) and $(10\bar{1})$, propagate between the TiS_3 chains, while $(90\bar{2})$, which is nearly perpendicular to the (001) plane, dissect the TiS_3 chains. This is further illustrated by Figure 3b, which demonstrates additional views of the TiS_3 crystal structure orthogonal to (100), (101) and $(10\bar{1})$ planes; the figure shows that these planes separate TiS_3 chains and do not dissect any of the covalent Ti-S bonds. For the sake of comparison, we also considered the (010) plane, which is perpendicular to the crystallographic *b* direction and cuts the TiS_3 chains.

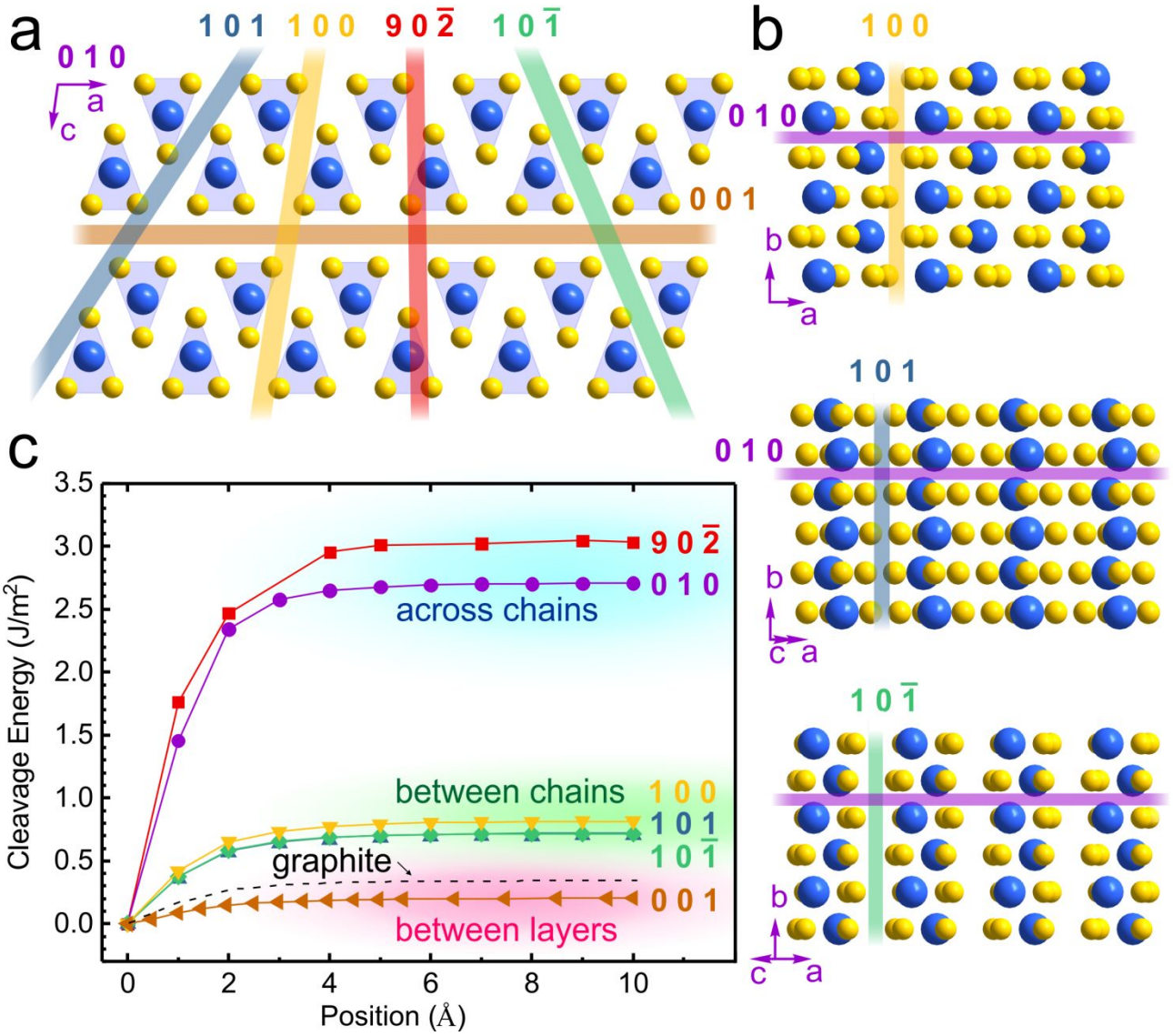

Figure 3. Cleavage energy calculations for different crystallographic planes in TiS_3. **(a)** Scheme of the planes in the TiS_3 structure that were considered for cleavage energy calculations. **(b)** Additional views of the TiS_3 along selected crystallographic directions showing that the (100), (101) and $(10\bar{1})$ planes separate TiS_3 chains and do not dissect any of the covalent Ti-S bonds, unlike the (010) plane. **(c)** Cleavage energies for various scenarios from (a,b) plotted as a function of the separation between the planes.

The results of the cleavage energy calculations for these crystallographic planes are shown in Figure 3c. The lowest cleavage energy was found for the (001) planes, which separate the 2D TiS_3 layers.

As shown in Figure 3c, the energy increases with the separation between the layers and converges to 0.204 J m^{-2}. As noted in the previous report,[15] this energy is lower than the cleavage energy for graphene layers in graphite crystal, which is shown by the dashed line in Figure 3c and converges at about 0.320 J m^{-2}. This computational result suggests that the exfoliation of 2D layers of TiS_3 crystals should be even easier than the exfoliation of graphene from graphite. Figure 3c also shows that other planes that separate the TiS_3 chains without dissecting the covalent Ti-S bonds have comparable cleavage energies converging at 0.714, 0.716 and 0.815 J/m^2 for the (101), $(10\bar{1})$ and (100) planes, respectively. These values are only about twice as large as the cleavage energies of graphite, suggesting that the mechanical exfoliation separating TiS_3 chains without breaking them is highly feasible. On the contrary, the planes that dissect the covalent bonds within the TiS_3 chains were found to have much higher cleavage energies, such as 2.706 J/m^2 for the (010) plane and 3.03 J/m^2 for the $(90\bar{2})$ plane (Figure 3c). Overall, the calculations show that breaking the weak bonding interactions between the 2D layers and between 1D chains within the layers require comparable energies, which in turn are considerably lower than those required for breaking the covalent bonds within the chains. These computational results agree well with the experimentally observed exfoliation of TiS_3, as the ease of cleavage between the 1D chains is consistent with the stripy pattern in the AFM image (Figure 2c). Also, the stripes have uniform widths, because as the cleavage starts in the crystallographic *b* direction between the chains it is unlikely to deviate in the *a* direction since breaking covalent bonds within the chains requires higher energy. The ease of cleavage between the 1D chains is also consistent with the very smooth and straight edges of the exfoliated TiS_3 nanoribbons.

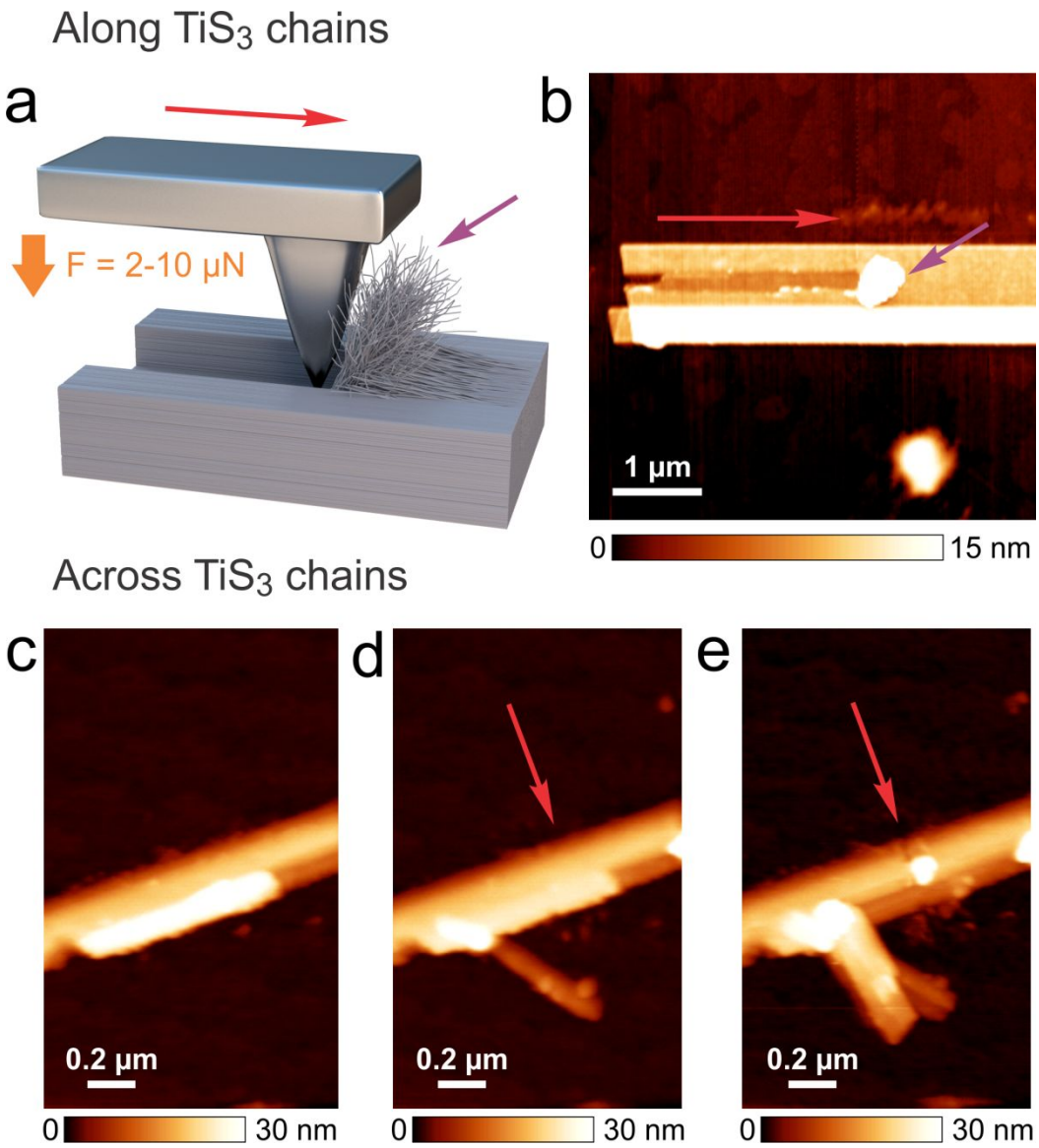

Figure 4. Nanomechanical exfoliation of TiS_3 crystals using AFM tip**. (a)** Scheme of TiS_3 cleavage using an AFM tip. **(b)** AFM image of a TiS_3 crystal on a barium titanite ($BaTiO_3$) substrate which was cleaved by an AFM tip along the 1D chains. Tip force: ≈10 μN. **(c-e)** AFM images of a TiS_3 crystal on a BTO substrate that was cleaved across the 1D chains: (c) as-prepared crystal, (d) the same crystal after the first cleavage (tip force: ≈2 μN) and (e) the same crystal after the second cleavage (tip force: ≈3 μN). The red arrows show the AFM tip cleavage directions.

While the mechanical exfoliation of the layered materials is usually performed on the macroscale by the manual peeling of crystals using an adhesive tape, it can also be realized on a nanoscale using an AFM tip. Figure 4a shows scheme of the experiment, in which a diamond tip is pressed against a TiS_3 crystal with a force of 2-10 μN and then dragged either along or across the direction of 1D chains. Figure 4b shows AFM image of a TiS_3 crystal, which was scratched in the direction marked by the red arrow. The moving tip with a force of ≈10 μN cleaved the 1D chains from the underlying 2D layer and the surrounding chains within the layer, forming a well visible scratch. The chains are pushed forward and accumulated together in a structure indicated by the blue arrow in Figure 4b. This cleavage scenario is illustrated by Figure 4a, in which the tip does not move across the covalently bonded 1D chains that require relatively high energies for cleavage (Figure 3).

The situation changes, when the AFM tip scratches an exfoliated TiS_3 crystal along the *a* direction. Since diamond is much harder than TiS_3, it can also cut the 1D chains across if a sufficient force is applied to the tip, which we observed experimentally in some cases. However, Figure 4c-e shows another possible scenario, in which a tip moving across a TiS_3 nanoribbon causes top 2D layers slide relative to the bottom layer, again providing evidence for their weak bonding interaction. Figure 4c shows AFM image of a fragment of as-prepared TiS_3 crystal. Figure 4d shows that the first drag of an AFM tip across this crystal with a force of ≈2 μN causes the top 2D layers slide to the side, while the second tip drag along the same trajectory with a force of ≈3 μN cleaves more 2D layers in a similar manner (Figure 4e). Overall, the nanoscale cleavage experiments further demonstrate the ease with which TiS_3 crystals can be exfoliated along the weakly bound 2D layers as well as 1D chains.

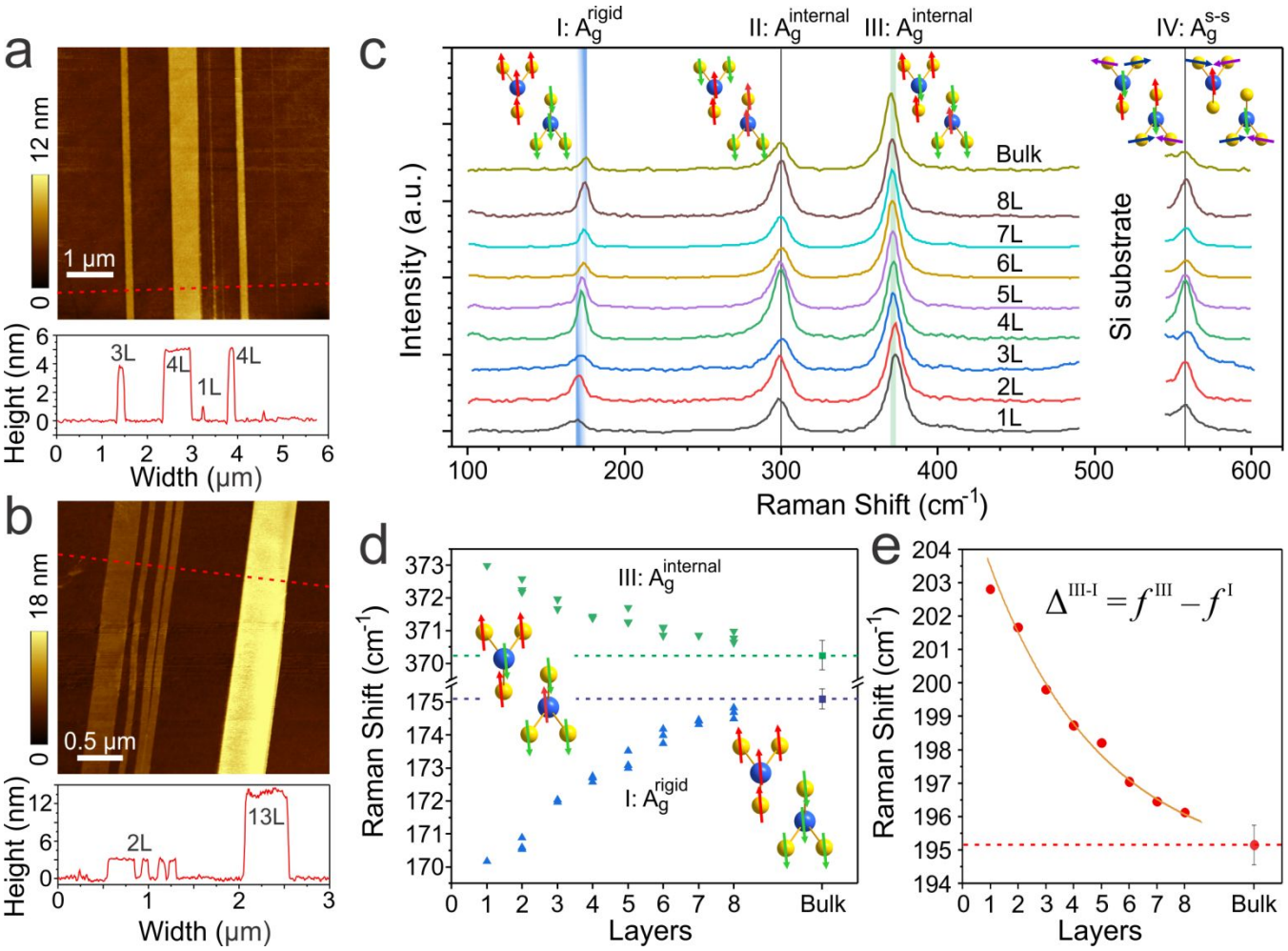

Figure 5. Thickness dependent Raman spectroscopy of TiS_3 flakes. **(a,b)** AFM images of TiS_3 nanoribbons of different thicknesses and the corresponding height profiles. **(c)** Raman spectra of exfoliated TiS_3 flakes with different number of monolayers. Raman-active optical modes are named according ref. 27 and are shown above the corresponding Raman peaks. **(d)** Frequencies f^{I} (▲) and f^{III} (▼) of I:A_g^{rigid} and III:$A_g^{internal}$ Raman-active modes, respectively, as a function of the number of layers in exfoliated TiS_3 crystals. Data points show frequencies from individual experiments. The peak positions for bulk crystals were averaged over 10 samples and are shown with error bars. **(e)** Averaged difference $\Delta^{III-I} = f^{III} - f^{I}$ of the frequencies of III:$A_g^{internal}$ and I:A_g^{rigid} Raman-active modes in TiS_3 as a function of the number of layers.

In the framework of this study, we exfoliated a large number of TiS_3 crystals with different thicknesses, which could be assessed by Raman spectroscopy. Several recent studies focused on understanding the origin and behavior of the Raman-active modes in TiS_3 and related TMTCs.[27-30] However, there is still a lack of information regarding the most common practical application of Raman spectroscopy to 2D materials, which is the determination of the number of monolayers in thin crystals. For example, Raman spectroscopy was shown to be a powerful tool for determining the number of monolayers in the most studied 2D materials, such as graphene,[31] hexagonal boron nitride,[32] MoS_2[33,34] and WS_2,[35] but information on how to distinguish between monolayer and few-layer TiS_3 crystals is still missing in literature.

There are several experimental complications for the Raman spectroscopy investigation of TiS_3 crystals with different thicknesses. First of all, since many exfoliated TiS_3 crystals have terraced surfaces, as shown in Figure 2c and Figure S6, they cannot be characterized by a specific number of layers. Second, since the splitting between the TiS_3 chains is nearly as easy as the splitting between the TiS_3 layers, during the exfoliation process the crystals typically not only get thinner but also narrower and often become too narrow for Raman spectroscopy. Monolayer (1L) TiS_3 nanoribbon that is only a few nm wide can be seen in Figure 5a. The observation of such narrow ribbons is interesting in the view of their potential application in nanoscale electronic devices, but characterization of such narrow TiS_3 crystals by conventional Raman microscopy with a focused laser beam spot of about 1 μm is problematic. In this study, we were able to identify a sufficient number of TiS_3 nanoribbons that had smooth surfaces and were wide enough for Raman spectroscopy. Examples of TiS_3 crystals with thicknesses up to 13 layers (13L) are shown in Figure 5a,b. The numbers of layers in these and similar images were assigned based on the entire set of AFM data. In the AFM images, monolayers of layered 2D materials often exhibit larger thickness in comparison with the expected theoretical thicknesses, which is attributed to the presence of water adsorbates and other

contaminants underneath.[1,36] In our AFM experiments, monolayer TiS_3 crystals were about 2 nm thick, and the thickness of TiS_3 crystals was increasing by ~0.9 nm per every additional layer.

Typical Raman spectra of TiS_3 flakes are shown in Figure 5c. The range from 490 to 530 cm^{-1} is not included, since the peaks from silica substrate are relatively strong due to thin and narrow sizes of TiS_3 flakes. We observed four A_g Raman-active modes near $f^{I} = 175$ cm^{-1}, $f^{II} = 300$ cm^{-1}, $f^{III} = 370$ cm^{-1} and $f^{IV} = 560$ cm^{-1}, which correspond to I:A_g^{rigid}, II:$A_g^{internal}$, III:$A_g^{internal}$ and IV:$A_g^{S\text{-}S}$, respectively; the peaks were assigned based on the calculations by Wu *et al*.[27] The positions of two of the four observed peaks, f^{II} and f^{IV}, did not exhibit significant dependences on the number of layers. In II:$A_g^{internal}$ mode the vibrations occur out-of-plane, but both trigonal prismatic chain are moving collectively in the same direction, making intrachannel interactions dominant. The IV:$A_g^{S\text{-}S}$ corresponds to in-plane vibrations between S_2^{2-} atoms in the same trigonal prismatic chain, so interlayer interactions do not significantly affect the frequency of this mode. However, we found a considerable downshift of the frequency f^{I} of the I:A_g^{rigid} mode from 175 to 170 cm^{-1} with decreasing the number of layers. There was also a noticeable increase of the frequency f^{III} of the III: $A_g^{internal}$ mode from 370 to 373 cm^{-1} with the number of layers (Figure 5d). These two modes have two trigonal prismatic chains moving in the opposite directions showing dominance of the interchain interaction, which reflects the quasi-one-dimensional structure of TiS_3, similar to ZrS_3 and $ZrSe_3$.[28] Since the frequencies f^{I} and f^{III} shift in the opposite directions with increasing the thickness of TiS_3, it is convenient to use their difference $\Delta^{III\text{-}I} = f^{III} - f^{I}$ to distinguish the number of layers in thin TiS_3 crystals (Figure 5e). A similar approach was successfully used for monolayer and few-layer MoS_2 flakes.[33,34] The $\Delta^{III\text{-}I}$ peak difference varies in a wider range (from 195 to 203 cm^{-1}) than any of the individual peaks, and while the positions of the individual peaks should be carefully measured versus a calibrated standard, the use of their difference eliminates systematic measurement errors.

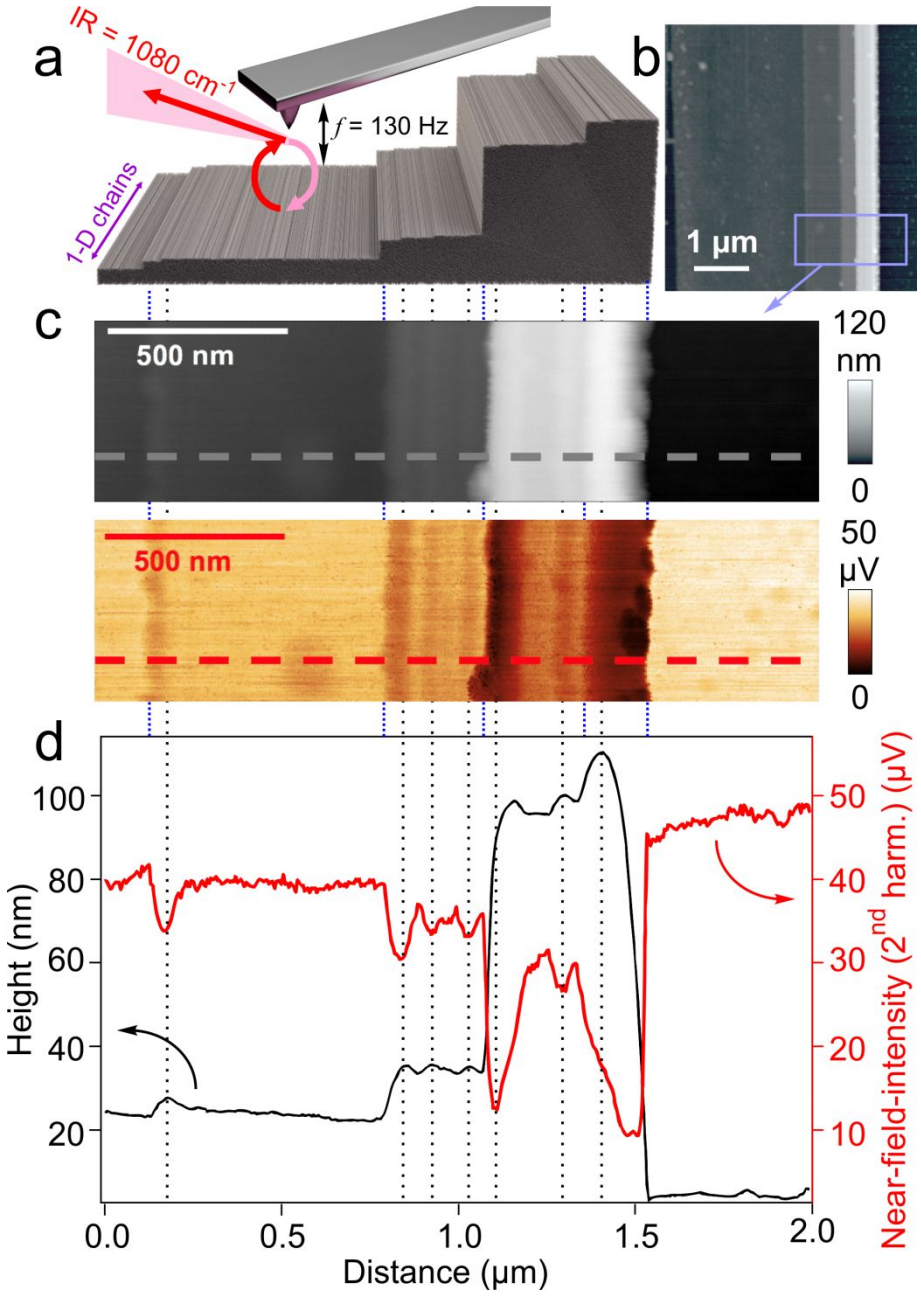

Figure 6. Scanning near-field optical microscopy of exfoliated TiS_3 flakes. **(a)** Scheme of the operation principle of the s-SNOM with incident laser-light scattered at the tip's apex, locally exciting the sample. The tip is oscillating at 130 kHz and collecting the chemical contrast simultaneously with the topography, while scanning the sample's surface. **(b)** Topography map from an AFM scan over an exfoliated TiS_3 crystal on Si/SiO_2. **(c)** High-resolution scan from the blue-marked area in (b), showing the topography of the step-like structure (top) of the TiS_3 surface and the near-filed-intensity map (bottom) collected laser

radiation operating at 9.261 μm (1080 cm^{-1}) at the second harmonic of the tip's oscillation frequency. **(d)** Cross section lines representing the topography (black) and the near-field intensity (red) across the TiS_3 steps shown in (c). Step edges (dashed blue lines) and other topographic features, corresponding the IR absorption (dashed black lines) are indicated.

Finally, we investigated exfoliated TiS_3 crystals on Si/SiO_2 by infrared (IR) scattering-type scanning near-field optical microscopy using an s-SNOM system that is schematically shown in Figure 6a. The system includes an atomic force microscope operated in the tapping mode and an asymmetric Michelson interferometer. Incident IR radiation of CO_2 gas laser is scattered on Au-coated silicon AFM cantilever which have resonance frequencies of around 130 kHz. In this experiment, simultaneously to the topography, we measured the IR response from the broad SiO_2 substrate phonon (ranging from 900 cm^{-1} to 1250 cm^{-1}) through the exfoliated TiS_3 crystal shown in the AFM image in Figure 6b. The near-field intensity maps were collected at 1080 cm^{-1}, the shortest wavenumber that is still accessible by the CO_2 laser. By tuning to off-resonance we avoided artefacts from the peak shifts due to sample-substrate interactions, as reported in previous near-field spectroscopic studies in the mid-infrared regime.[37,38] The spectroscopic response did not include a signal from the TiS_3 crystal, which shows infrared features at wavenumbers well below 450 cm^{-1}, the spectral range that is not accessible to the used light source and is below the detector's sensitivity range.

In Figure 6c, a high-resolution scan of size 2 μm x 0.25 μm which represents the marked blue area shown in Figure 6b. The upper part of Figure 6c is a topographic representation of the TiS_3 whisker while the bottom part is a near-field intensity map collected at second harmonic of the tip oscillation frequency. For a clearer view the cross-section lines at the position marked by dashed black and red lines (Figure 6c) are shown. In Figure 6d the black line represents the topography of the sample and the red line corresponds

to the simultaneously taken near-field signal. Clearly, the near field intensity drops at the positions of the edges of the TiS_3 whisker terraces. The intensity attenuation is not constant along the entire TiS_3 step structure and slightly recovers towards the next terrace and drops again in the presence of another edge. Additionally, the near-field signal intensity drop is deeper depending on the height difference between the involved terraces. As mentioned above, the near field signal at 1080 cm^{-1} is characteristic for the underlying SiO_2 substrate and is due to the strong optical response from the SiO_2 phonon resonance peaking at 1130 cm^{-1}. The intensity of the near-field response originating from the SiO_2 phonon is strongly dependent on the tip-sample interactions. The presence of TiS_3 on top of SiO_2 is directly affecting the coupling of the infrared radiation focused by the tip to the SiO_2 phonon, which results in near-field intensity drops, leading to strong discontinuities at the terrace edges. However, in the optical intensity signal, these strong discontinuities are not restricted just to edges, but propagate well into terraces, suggesting that this effect is strongest at the terrace edge, but also affects the terraces. Considering the TiS_3 crystal structure and the appearance of the exfoliated nanoribbons in Figure 2c, the suppressions of the substrate phonon responses near the edges of crystal terraces in s-SNOM measurements are consistent with the uniform sulfur termination of the quasi-1D TiS_3 chains.

In summary, the TiS_3 nanoribbons with straight and smooth edges showing clear signatures of 1D chains were produced by micromechanical exfoliation. The observed structures form due to the drastically different cleavage energies for various crystallographic planes. The theoretical calculations show that breaking weak interactions between the 2D layers and between 1D chains within the layers require comparable energies, which in turn are considerably higher than those required for breaking the covalent bonds within the chains. The macroscopic exfoliation experiments were emulated on the nanoscale by applying a local shear force along the different crystallographic directions using an AFM tip. In the AFM experiments it was both possible to slide the 2D TiS_3 layers relative to each other or remove selected 1D

chains from the layers. We systematically studied the exfoliated TiS_3 crystals by Raman spectroscopy and demonstrate which Raman peaks are most dependent on the crystals' thickness. These results could be used to distinguish between TiS_3 crystals with thicknesses ranging from one to about seven monolayers. Finally, we used nano-infrared near-field microscopy showing a decrease of the nearfield intensity signal near the terrace edges slowly recovering towards the center of the terrace, which we relate to the edge charge accumulation combined with Coulomb repulsion, which consistent with the expected uniform sulfur termination at the edges and terraces in the TiS_3 crystals. The conclusions established in this study for the exfoliated TiS_3 crystals can likely be extended to other TMTC materials as well as other quasi-1D crystals. The possibility of exfoliation of TiS_3 into crystals with smooth edges could be important for the future realization of miniature 2D device channels with reduced edge scattering.

Experimental Methods

Cleavage energies calculations

The cleavage energies calculations are carried out using density functional theory (DFT) methods within the generalized gradient approximation (GGA) and with the Perdew–Burke–Ernzerhof (PBE) exchange correlation functional, as implemented in the Vienna *ab initio* simulation package (VASP).[39] The Grimme's D3 dispersion correction is adopted to account for the long-range interactions. The ion–electron interaction is treated using the projector-augment-wave (PAW) technique and a kinetic energy cut of 500 eV is chosen. The cleavage is simulated by introducing a fracture in the TiS_3 ribbon where the edges are passivated with hydrogen. The total energies under variation of the separation between the fractured parts are computed to simulate the cleavage process.

Transmission Electron Microscopy (TEM)

The microstructure of TiS_3 flakes was studied using a FEI Tecnai Osiris scanning transmission electron microscope equipped with a HAADF detector and a X-FEG high brightness Schottky field emission gun. The accelerating voltage was 200 kV.

Exfoliation by AFM tip

The cleavage experiment was done on a commercial AFM system (MFP3D, Asylum Research). Diamond coated AFM tips (CDT-NCHR, Nanosensors) with a spring constant about 40 N/m was used to perform cleavage on the TiS_3 crystals.

Infrared scattering-type near-field optical microscopy (s-SNOM)

The experimental setup has been described before in detail.[38,40,41] It consists of a commercial scattering-type SNOM (s-SNOM) system (NeaSNOM, Neaspec GmbH, Germany), which includes an atomic force microscope operated in the tapping mode and an asymmetric Michelson interferometer. Au-coated silicon AFM cantilevers with a gold metal layer of about 30 nm thickness and resonance frequencies of around 130 kHz were used as a scattering element of the microscope. The average tip diameter of near-field probes was below 50 nm. As for the IR radiation sources, we used a grating tuned CO_2 gas laser (PL5, Edinburgh Instruments, UK) operating in sealed-off mode. This source is characterized by high intensity and frequency stability within a limited spectral range, which can be regarded as a suitable tool for nano-imaging experiments at discrete wavelengths.

Raman spectroscopy

Raman spectra were measured at room temperature with a Thermo Scientific DXR Raman microscope operated in normal incidence and back-scattered configuration. A solid laser of $\lambda = 532$ nm was used as excitation light, and typical laser power was kept at 0.1 mW to prevent thermal damage to the flakes. Si band at 520 cm^{-1} was used as a frequency reference. The spectral resolution was 0.96 cm^{-1}. The laser was focused through a 100x objective with laser spot size of about 2 μm on the sample.

ASSOCIATED CONTENT

Supporting Information.

The Supporting Information is available free of charge on the ACS Publications website at DOI: 10.1021/

Scheme of TiS_3 synthesis; X-ray photoelectron spectroscopy (XPS) analysis; Energy-dispersive x-ray (EDX) spectrum, additional TEM and selected area electron diffraction (SAED) images; SEM images; additional AFM images (PDF)

AUTHOR INFORMATION

Corresponding Author

*E-mail: sinitskii@unl.edu

Author Contributions

The manuscript was written through contributions of all authors. All authors have given approval to the final version of the manuscript.

Acknowledgements:

This research was supported by the National Science Foundation, through grants NSF ECCS-1740136 and ECCS-1508541, the nCORE, a wholly owned subsidiary of the Semiconductor Research Corporation (SRC), and the Nebraska Materials Research Science and Engineering Center (MRSEC) (NSF DMR-1420645). The materials characterization was performed in part in MISIS, in which the work was supported by the Ministry of Education and Science of the Russian Federation (K2-2018-014), and in the Nebraska Nanoscale Facility, which is supported by the NSF (ECCS-1542182) and the Nebraska Research

Initiative. Financial support by the German Research Foundation (DFG) within SFB 1112 (TP B02) is also gratefully acknowledged.

REFERENCES

1. Novoselov, K. S.; Jiang, D.; Schedin, F.; Booth, T. J.; Khotkevich, V. V.; Morozov, S. V.; Geim, A. K. Two-Dimensional Atomic Crystals. *Proc. Natl. Acad. Sci. U. S. A.* **2005**, *102*, 10451-10453.
2. Geim, A. K.; Grigorieva, I. V. Van der Waals Heterostructures. *Nature* **2013**, *499*, 419-425.
3. Butler, S. Z.; Hollen, S. M.; Cao, L.; Cui, Y.; Gupta, J. A.; Gutiérrez, H. R.; Heinz, T. F.; Hong, S. S.; Huang, J.; Ismach, A. F.; Johnston-Halperin, E.; Kuno, M.; Plashnitsa, V. V.; Robinson, R. D.; Ruoff, R. S.; Salahuddin, S.; Shan, J.; Shi, L.; Spencer, M. G.; Terrones, M.; Windl, W.; Goldberger, J. E. Progress, Challenges, and Opportunities in Two-Dimensional Materials Beyond Graphene. *ACS Nano* **2013**, *7*, 2898-2926.
4. Bhimanapati, G. R.; Lin, Z.; Meunier, V.; Jung, Y.; Cha, J.; Das, S.; Xiao, D.; Son, Y.; Strano, M. S.; Cooper, V. R.; Liang, L.; Louie, S. G.; Ringe, E.; Zhou, W.; Kim, S. S.; Naik, R. R.; Sumpter, B. G.; Terrones, H.; Xia, F.; Wang, Y.; Zhu, J.; Akinwande, D.; Alem, N.; Schuller, J. A.; Schaak, R. E.; Terrones, M.; Robinson, J. A. Recent Advances in Two-Dimensional Materials beyond Graphene. *ACS Nano* **2015**, *9*, 11509-11539.
5. Furuseth, S.; Brattas, L.; Kjekshus, A. On the Crystal Structures of TiS_3, ZrS_3, $ZrSe_3$, $ZrTe_3$, HfS_3, and $HfSe_3$. *Acta Chemica Scandinavica A* **1975**, *29*, 623-631.
6. Srivastava, S. K.; Avasthi, B. N. Preparation, structure and properties of transition metal trichalcogenides. *J. Mater. Sci.* **1992**, *27*, 3693-3705.

7. Dai, J.; Li, M.; Zeng, X. C. Group IVB transition metal trichalcogenides: a new class of 2D layered materials beyond graphene. *Wiley Interdisciplinary Reviews: Computational Molecular Science* **2016**, *6*, 211-222.
8. Island, J. O.; Molina-Mendoza, A. J.; Barawi, M.; Biele, R.; Flores, E.; Clamagirand, J. M.; Ares, J. R.; Sánchez, C.; van der Zant, H. S.; D'Agosta, R.; Ferrer, I. J.; Castellanos-Gomez, A. Electronics and optoelectronics of quasi-1D layered transition metal trichalcogenides. *2D Materials* **2017**, *4*, 022003.
9. Yi, H.; Komesu, T.; Gilbert, S.; Hao, G.; Yost, A. J.; Lipatov, A.; Sinitskii, A.; Avila, J.; Chen, C.; Asensio, M. C.; Dowben, P. A. The band structure of the quasi-one-dimensional layered semiconductor TiS_3(001). *Appl. Phys. Lett.* **2018**, *112*, 052102.
10. Finkman, E.; Fisher, B. Electrical transport measurements in TiS_3. *Solid State Commun.* **1984**, *50*, 25-28.
11. Ferrer, I. J.; Ares, J. R.; Clamagirand, J. M.; Barawi, M.; Sánchez, C. Optical properties of titanium trisulphide (TiS_3) thin films. *Thin Solid Films* **2013**, *535*, 398-401.
12. Murphy, D. W.; Trumbore, F. A. Chemistry of TiS_3 and $NbSe_3$ Cathodes. *J. Electrochem. Soc.* **1976**, *123*, 960-964.
13. Zanini, M.; Shaw, J. L.; Tennenhouse, G. J. The Behavior of Na-TiS_2 and Na-TiS_3 as Solid-Solution Electrodes. *J. Electrochem. Soc.* **1981**, *128*, 1647-1650.
14. Hayashi, A.; Matsuyama, T.; Sakuda, A.; Tatsumisago, M. Amorphous Titanium Sulfide Electrode for All-solid-state Rechargeable Lithium Batteries with High Capacity. *Chem. Lett.* **2012**, *41*, 886-888.

15. Dai, J.; Zeng, X. C. Titanium Trisulfide Monolayer: Theoretical Prediction of a New Direct-Gap Semiconductor with High and Anisotropic Carrier Mobility. *Angewandte Chemie International Edition* **2015**, *54*, 7572-7576.

16. Kang, J.; Sahin, H.; Ozaydin, H. D.; Senger, R. T.; Peeters, F. M. TiS_3 nanoribbons: Width-independent band gap and strain-tunable electronic properties. *Phys. Rev. B* **2015**, *92*, 075413.

17. Zhang, J.; Liu, X.; Wen, Y.; Shi, L.; Chen, R.; Liu, H.; Shan, B. Titanium Trisulfide Monolayer as a Potential Thermoelectric Material: A First-Principles-Based Boltzmann Transport Study. *ACS Appl. Mater. Interfaces* **2017**, *9*, 2509-2515.

18. Morozova, N. V.; Korobeinikov, I. V.; Kurochka, K. V.; Titov, A. N.; Ovsyannikov, S. V. Thermoelectric Properties of Compressed Titanium and Zirconium Trichalcogenides. *The Journal of Physical Chemistry C* **2018**, *122*, 14362-14372.

19. Haraldsen, H.; Rost, E.; Kjekshus, A.; Steffens.A On Properties of TiS_3, ZrS_3, and HfS_3. *Acta Chem. Scand.* **1963**, *17*, 1283-&.

20. Brattas, L.; Kjekshus, A. On the Properties of Compounds with the $ZrSe_3$ Type Structure. *Acta Chem. Scand.* **1972**, *26*, 3441-3449.

21. Island, J. O.; Buscema, M.; Barawi, M.; Clamagirand, J. M.; Ares, J. R.; Sánchez, C.; Ferrer, I. J.; Steele, G. A.; van der Zant, H. S. J.; Castellanos-Gomez, A. Ultrahigh Photoresponse of Few-Layer TiS_3 Nanoribbon Transistors. *Advanced Optical Materials* **2014**, *2*, 641-645.

22. Lipatov, A.; Wilson, P. M.; Shekhirev, M.; Teeter, J. D.; Netusil, R.; Sinitskii, A. Few-Layered Titanium Trisulfide (TiS_3) Field-Effect Transistors. *Nanoscale* **2015**, *7*, 12291-12296.

23. Island, J. O.; Barawi, M.; Biele, R.; Almazán, A.; Clamagirand, J. M.; Ares, J. R.; Sánchez, C.; van der Zant, H. S. J.; Álvarez, J. V.; D'Agosta, R.; Ferrer, I. J.; Castellanos-Gomez, A. TiS_3 Transistors with Tailored Morphology and Electrical Properties. *Adv. Mater.* **2015**, *27*, 2595-2601.

24. Wang, M.; Li, C. M. Excitonic properties of graphene-based materials. *Nanoscale* **2012**, *4*, 1044-1050.

25. Cui, Q.; Lipatov, A.; Wilt, J. S.; Bellus, M. Z.; Zeng, X. C.; Wu, J.; Sinitskii, A.; Zhao, H. Time-Resolved Measurements of Photocarrier Dynamics in TiS_3 Nanoribbons. *ACS Appl. Mater. Interfaces* **2016**, *8*, 18334-18338.

26. Molina-Mendoza, A. J.; Island, J. O.; Paz, W. S.; Clamagirand, J. M.; Ares, J. R.; Flores, E.; Leardini, F.; Sánchez, C.; Agraït, N.; Rubio-Bollinger, G.; van der Zant, H. S. J.; Ferrer, I. J.; Palacios, J. J.; Castellanos-Gomez, A. High Current Density Electrical Breakdown of TiS_3 Nanoribbon-Based Field-Effect Transistors. *Adv. Funct. Mater.* **2017**, *27*, 1605647.

27. Wu, K.; Torun, E.; Sahin, H.; Chen, B.; Fan, X.; Pant, A.; Parsons Wright, D.; Aoki, T.; Peeters, F. M.; Soignard, E.; Tongay, S. Unusual lattice vibration characteristics in whiskers of the pseudo-one-dimensional titanium trisulfide TiS_3. *Nat. Commun.* **2016**, *7*, 12952.

28. Osada, K.; Bae, S.; Tanaka, M.; Raebiger, H.; Shudo, K.; Suzuki, T. Phonon Properties of Few-Layer Crystals of Quasi-One-Dimensional ZrS_3 and $ZrSe_3$. *The Journal of Physical Chemistry C* **2016**, *120*, 4653-4659.

29. Kong, W.; Bacaksiz, C.; Chen, B.; Wu, K.; Blei, M.; Fan, X.; Shen, Y.; Sahin, H.; Wright, D.; Narang, D. S.; Tongay, S. Angle resolved vibrational properties of anisotropic transition metal trichalcogenide nanosheets. *Nanoscale* **2017**, *9*, 4175-4182.

30. Pawbake, A. S.; Island, J. O.; Flores, E.; Ares, J. R.; Sanchez, C.; Ferrer, I. J.; Jadkar, S. R.; van der Zant, H. S. J.; Castellanos-Gomez, A.; Late, D. J. Temperature-Dependent Raman Spectroscopy of Titanium Trisulfide (TiS_3) Nanoribbons and Nanosheets. *ACS Appl. Mater. Interfaces* **2015**, *7*, 24185-24190.

31. Ferrari, A. C.; Meyer, J. C.; Scardaci, V.; Casiraghi, C.; Lazzeri, M.; Mauri, F.; Piscanec, S.; Jiang, D.; Novoselov, K. S.; Roth, S.; Geim, A. K. Raman Spectrum of Graphene and Graphene Layers. *Phys. Rev. Lett.* **2006**, *97*, 187401.

32. Gorbachev, R. V.; Riaz, I.; Nair, R. R.; Jalil, R.; Britnell, L.; Belle, B. D.; Hill, E. W.; Novoselov, K. S.; Watanabe, K.; Taniguchi, T.; Geim, A. K.; Blake, P. Hunting for Monolayer Boron Nitride: Optical and Raman Signatures. *Small* **2011**, *7*, 465-468.

33. Li, H.; Zhang, Q.; Yap, C. C. R.; Tay, B. K.; Edwin, T. H. T.; Olivier, A.; Baillargeat, D. From Bulk to Monolayer MoS_2: Evolution of Raman Scattering. *Adv. Funct. Mater.* **2012**, *22*, 1385-1390.

34. Lee, C.; Yan, H.; Brus, L. E.; Heinz, T. F.; Hone, J.; Ryu, S. Anomalous Lattice Vibrations of Single- and Few-Layer MoS_2. *ACS Nano* **2010**, *4*, 2695-2700.

35. Berkdemir, A.; Gutiérrez, H. R.; Botello-Méndez, A. R.; Perea-López, N.; Elías, A. L.; Chia, C.-I.; Wang, B.; Crespi, V. H.; López-Urías, F.; Charlier, J.-C.; Terrones, H.; Terrones, M. Identification of individual and few layers of WS_2 using Raman Spectroscopy. *Scientific Reports* **2013**, *3*, 1755.

36. Lipatov, A.; Lu, H.; Alhabeb, M.; Anasori, B.; Gruverman, A.; Gogotsi, Y.; Sinitskii, A. Elastic properties of 2D $Ti_3C_2T_x$ MXene monolayers and bilayers. *Science Advances* **2018**, *4*, eaat0491.

37. Amarie, S.; Keilmann, F. Broadband-infrared assessment of phonon resonance in scattering-type near-field microscopy. *Phys. Rev. B* **2011**, *83*, 045404.

38. Patoka, P.; Ulrich, G.; Nguyen, A. E.; Bartels, L.; Dowben, P. A.; Turkowski, V.; Rahman, T. S.; Hermann, P.; Kästner, B.; Hoehl, A.; Ulm, G.; Rühl, E. Nanoscale plasmonic phenomena in CVD-grown MoS_2 monolayer revealed by ultra-broadband synchrotron radiation based nano-FTIR spectroscopy and near-field microscopy. *Optics Express* **2016**, *24*, 1154-1164.

39. Kresse, G.; Furthmuller, J. Efficient iterative schemes for ab initio total-energy calculations using a plane-wave basis set. *Phys. Rev. B* **1996**, *54*, 11169-11186.

40. Hermann, P.; Hoehl, A.; Patoka, P.; Huth, F.; Rühl, E.; Ulm, G. Near-field imaging and nano-Fourier-transform infrared spectroscopy using broadband synchrotron radiation. *Optics Express* **2013**, *21*, 2913-2919.

41. Hermann, P.; Hoehl, A.; Ulrich, G.; Fleischmann, C.; Hermelink, A.; Kästner, B.; Patoka, P.; Hornemann, A.; Beckhoff, B.; Rühl, E.; Ulm, G. Characterization of semiconductor materials using synchrotron radiation-based near-field infrared microscopy and nano-FTIR spectroscopy. *Optics Express* **2014**, *22*, 17948-17958.

TOC graphic

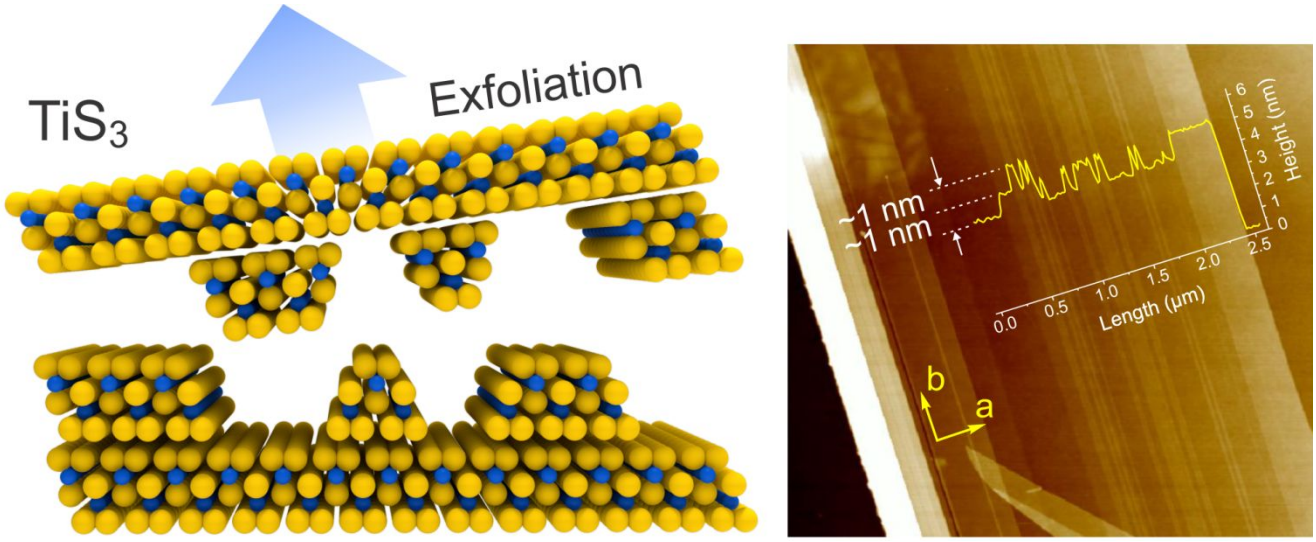
TiS3
Exfoliation
~1 nm
~1 nm
Height (nm)
Length (μm)
0.0
0.5
1.0
1.5
2.0
2.5
b
a